Hardware-in-the-Loop Methods for Stability Analysis of Multiple Parallel Inverters in Three-Phase AC Systems

Henrik Alenius, *Member, IEEE*, Tomi Roinila, *Member, IEEE*, Roni Luhtala, *Member, IEEE*, Tuomas Messo, *Member, IEEE*, Andrew Burstein, *Member, IEEE*, Erik de Jong, *Senior Member, IEEE*, and Alejandra Fabian

***Abstract*— Modern electric distribution systems typically contain several feedback-controlled parallel inverters that together form a complex power distribution system. Consequently, a number of issues related to stability arise due to interactions among multiple inverter subsystems. Recent studies have presented methods where the stability and other dynamic characteristics of a paralleled inverter system can be effectively analyzed using impedance measurements. This article presents implementation techniques for comprehensive online stability analysis of grid-connected paralleled inverters using power hardware-in-the-loop measurements based on an OPAL-RT real-time simulator. The analysis is based on simultaneous online measurements of current control loop gains of the inverters and the grid impedance, and aggregated terminal admittance measurements of the inverters. The analysis includes the measurement of the inverters' aggregated output impedance, inverters' loop gains, global minor loop gain, and grid impedance. The presented methods make it possible to rapidly evaluate the system on both global and local levels in real time, thereby providing means for online stability monitoring or adaptive control of such systems. Experimental measurements are shown from a high-power energy distribution system recently developed at DNV GL, Arnhem, The Netherlands.**

***Index Terms*— Frequency-domain analysis, parallel inverters, power system stability, stability analysis, three-phase electric power.**

I. Introduction

AN INCREASING number of applications of ac-distributed power systems have been made possible due to advances in semiconductor technologies and inverter topologies. These applications can be found in several new and emerging fields, including renewable energy generation [1], hybrid and electric vehicles [2], smart grids [3], electric aircraft [4], and electric ships [5].

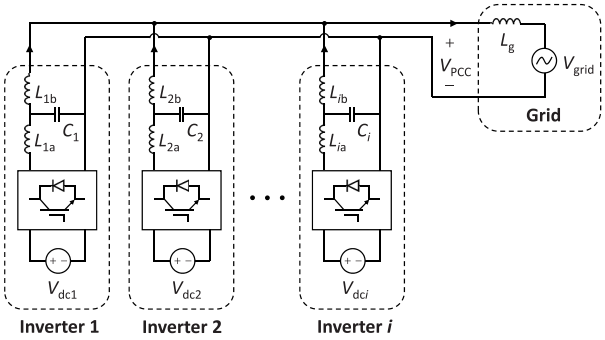

Fig. 1. Parallel grid-connected inverters.

The ac-distributed power systems are most often dependent on the operation of paralleled inverters. In some applications, such as large-scale photovoltaic or wind power plants, the system may include hundreds or even thousands of inverters operating in parallel for scaling up the total power generation capacity. Fig. 1 shows a typical configuration of multiparalleled inverters connected to a power grid through a point of common coupling (PCC). Usually, the inverters are individually designed based on the stability requirements of the inverter standalone operation. However, the use of multiple inverters in parallel results in dynamic interaction causing system performance degradation or even instability [6], as reported from distribution systems that include photovoltaic plants [7], wind power systems [8], [9], and data centers [10].

Stability issues involved in multiparalleled grid-connected inverters have been studied extensively in recent years. In [11], a small-signal stability assessment method was presented, where the stability is assessed based on the outermost voltage and frequency droops while neglecting the inner controller dynamics. The work in [12] presented a method in which multiple paralleled inverters were modeled as a multivariable system, where an equivalent inverter described the totality of multiple inverters. The work in [12] was based on the hypothesis that all the current references for each inverter are the same. However, considering that the reference of each inverter is independently controlled, such as in a PV plant where current references vary along

Manuscript received March 23, 2020; revised July 3, 2020 and July 29, 2020; accepted August 3, 2020. Date of publication August 6, 2020; date of current version December 1, 2021. This work was supported in part by the European Union's Horizon 2020 Research and Innovation Programme under Grant Agreement 654113 and in part by the Academy of Finland. Recommended for publication by Associate Editor John Fletcher. *(Corresponding author: Henrik Alenius.)*

Henrik Alenius and Tuomas Messo are with the Faculty of Information Technology and Communication Sciences, Tampere University, 33100 Tampere, Finland (e-mail: henrik.alenius@tuni.fi; tuomas.messo@tuni.fi).

Tomi Roinila and Roni Luhtala are with the Faculty of Engineering and Natural Sciences, Tampere University, 33100 Tampere, Finland (e-mail: tomi.roinila@tuni.fi; roni.luhtala@tuni.fi).

Andrew Burstein, Erik de Jong, and Alejandra Fabian are with the DNV GL, 6812 Arnhem, The Netherlands (e-mail: andrew.burstein@dnvgl.com; erik.dejong@dnvgl.com; alejandra.fabian@dnvgl.com).

Color versions of one or more of the figures in this article are available online at https://ieeexplore.ieee.org.

Digital Object Identifier 10.1109/JESTPE.2020.3014665

with maximum-power-point-tracking algorithm, the presented model lacks some essential physical significance and cannot comprehensively describe the characteristics of a PV plant. Lu *et al.* [13] applied a similar approach and presented models based on interactive current and common current to describe the interaction among multiple paralleled inverters.

The impedance-based small-signal analysis provides another method to evaluate the system stability [14], [15]. In this method, the impedances of source and load subsystems are measured, and the Nyquist stability criterion is applied to assess the system stability. While this method is characterized by simplicity, it does not provide any information on the system's internal stability poles [16]. The system's internal stability was considered by Cavazzana *et al.* [17], which provided an interpretation of the stability analysis presented in [12] using the source and load impedances. An alternative method for the impedance-based analysis was presented in [18], where the stability of a grid-connected inverter was characterized by the measured load-affected current-controller loop.

In many modern distribution systems, the high share of renewable production combined with multiple parallel inverters introduces changes to the power system [19]. Especially, in microgrids, the system operation status and configuration may fluctuate along with changes in the loading state, power generation, or grid topology. As a consequence, it may become challenging to predict the detailed system characteristics required in most stability analysis methods. In highly fluctuating conditions, a stability analysis based on typical operation status may be insufficient. To tackle this issue, real-time analysis methods based on continuous online measurements are highly desirable. The real-time stability indications can be applied in advanced system monitoring, fault prevention, or adaptive control. The online identification and analysis can be integrated into the inverter controllers applying digital analyzer techniques [20], [21].

This article considers the real-time stability analysis of paralleled grid-connected inverters by utilizing an OPAL-RT power hardware-in-the-loop (PHIL) setup that was developed recently at DNV GL, Arnhem, The Netherlands. The OPAL-RT is a multipurpose real-time simulator that is widely used in real-time analysis and control of various power-electronics applications, including wind-turbine emulation [22], fuel-cell modeling [23], and analysis of smart-grid performance [24]. A PHIL setup consists of a hardware-in-the-loop simulator, such as OPAL-RT, and power hardware, such as physical power cables and devices [25]. Recently, PHIL setups have been applied in versatile experimenting of various power-electric systems [26]–[28].

The primary goal of this work is to provide detailed steps toward implementing a comprehensive real-time stability analysis for a system that has multiple paralleled inverters connected to a grid. The second goal of the work is to present the proof of concept for online stability analysis performed with parallel approaches simultaneously and to compare the obtained stability indications. The method includes simultaneous use of loop gain analysis and impedance-based analysis applying an online multivariable measurement. The concept is applied to an experimental system at a 50-kW power level.

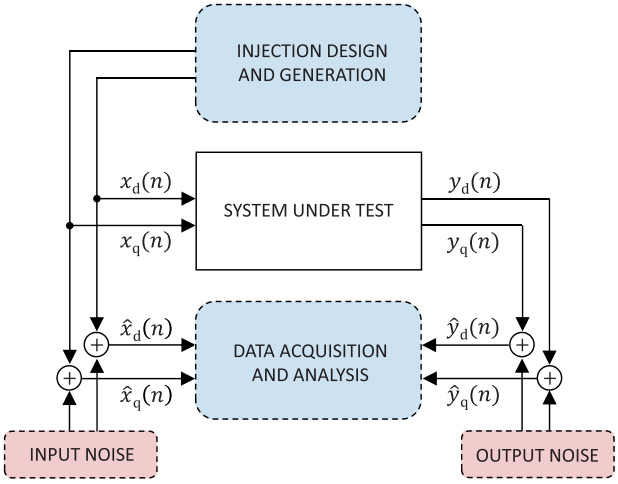

Fig. 2. Typical measurement setup.

The remainder of this article is organized as follows. Section II reviews the theory of the frequency-response identification using orthogonal wideband techniques applied in this article. Section III introduces the experimental high-power PHIL setup recently developed at DNV GL and presents the implementation of the online frequency-response measurement method. Section IV presents experimental results based on paralleled high-power inverters connected to a high-impedance grid and operated with different controller tunings. Finally, Section V draws conclusions.

II. Methods

A. Frequency-Response Measurement in the dq-Domain

Direct–quadrature (dq) transformation rotates the reference frame of three-phase systems in order to simplify the analysis of three-phase circuits. In the case of balanced three-phase circuits, the transformation reduces three ac quantities to two dc quantities, which makes it possible to utilize controllers with simpler structures and lower dynamic orders [29]. The dq-frame representation allows straightforward small-signal analysis as the nonlinear characteristics can be linearized around the steady-state operation point [30].

Fig. 2 shows a typical measurement setup where the system under test is to be identified in the dq-domain [31]. Examples of such identification include the output impedance of a three-phase inverter, inverter loop gain(s), and grid impedance [29]. In the setup, the system is perturbed by d- and q-component injections $x_d(n)$ and $x_q(n)$ that yield the corresponding output responses $y_d(n)$ and $y_q(n)$. The measured input and output signals, $[\hat{x}_d(n), \hat{x}_q(n)]$ and $[\hat{y}_d(n), \hat{y}_q(n)]$, are corrupted by input noise and output noise, respectively. The noise signals are assumed to resemble white noise and are uncorrelated with the other system variables. All the signals are assumed to be zero-mean sequences. The measured signals are buffered and segmented, and the signals are transformed to the frequency domain by applying discrete Fourier transformation (DFT), given as

$$\hat{X}(j\omega) = \mathcal{F}\{\hat{x}(n)\} \tag{1}$$

where $\hat{X}(j\omega)$ is the signal transformed to the frequency domain. From the Fourier-transformed input and output

signals, the frequency response (impedance or loop gain) can be obtained for each input/output pair by applying

$$G(j\omega) = \frac{\hat{Y}(j\omega)}{\hat{X}(j\omega)} \tag{2}$$

where $\hat{X}(j\omega)$ is the Fourier-transformed input signal and $\hat{Y}(j\omega)$ is the Fourier-transformed output signal. In impedance measurements, for example, the input is a current signal (containing the nominal current and injected current perturbation), and the output is the resulting voltage signal. In noisy environments, the logarithmic averaging procedure [31] is often applied to compute the frequency response between the desired variables as

$$G_{\log}(j\omega) = \left(\prod_{k=1}^{P} \frac{\hat{Y}_k(j\omega)}{\hat{X}_k(j\omega)} \right)^{1/P} \tag{3}$$

where P denotes the number of injected excitation periods. The method tends to cancel out the effect of uncorrelated noise from both input and output sides so that the frequency response is obtained more accurately compared with conventional cross correlation techniques [31]. In the dq-domain analysis, the method is applied to each input–output couple, resulting in a 2×2 frequency-response matrix that represents a frequency response from each input (input d- and q-components) to each output (output d- and q-components). That is, the matrix includes the direct components as well as the cross-coupling components.

B. Maximum-Length Binary Sequence

The perturbation design plays a very important role in obtaining the desired frequency response (or any other parametric or nonparametric system model) through the experiment described in Fig. 2. An optimal design leads to maximally informative experiments that extract the maximum amount of information and reduce operational costs associated with the identification procedure. For a linear-system identification of sensitive systems, a binary signal, such as maximum-length binary sequence (MLBS), most often offers the best possible choice in terms of maximizing signal power within time-domain-amplitude constraints [32]. The MLBS is a periodic broadband signal that has a largely controllable spectral energy distribution, and consequently, the measurements can be averaged over multiple periods to increase the signal-to-noise ratio [32]. The averaging procedure enables accurate online measurements even with very small injection amplitude, which may be a requirement in sensitive systems where large injection amplitude, such as in impulse injection, may disrupt the system operation. Another major advantage of the MLBS over the other types of signals, such as sinusoids, is that the sequence can be implemented with a low-cost system whose output can only generate a small number of signal levels. Due to the several favorable characteristics, the MLBS has become a popular perturbation signal in the stability analysis of both ac and dc power distribution systems [33]–[37].

C. Orthogonal Perturbations

Considering the multiple-input–multiple-output (MIMO) system in Fig. 2, the inputs and outputs are most often coupled.

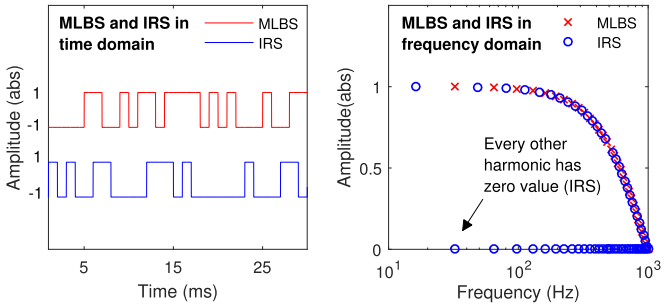

Fig. 3. Two orthogonal sequences (MLBS and IRS) in time and frequency domains.

For such a system, the conventional approach is to apply the superposition theorem to the frequency-response measurements, where the excitation signal is separately injected to each system input one at a time, and all the output responses are measured for each input excitation [31]. Then, (3) is applied to each combination of input and output. However, the superposition approach requires multiple consecutive measurements, which increases the measurement time and may make the results prone to variations in the system under measurement. In this work, the MIMO system is measured by applying orthogonal binary sequences, where multiple orthogonal injections are used to simultaneously excite all the system inputs. As the injections are orthogonal (that is, they have energy at different frequencies), the injections do not disturb each other, and the MIMO system can be identified simultaneously within one measurement cycle [38]. Consequently, the technique has considerable advantages over the method using superposition theorem and sequential perturbations, as all the frequency responses are measured simultaneously under the same system operation conditions.

The synthesis of orthogonal (periodic) binary sequences has been well documented [32]. One of the most popular techniques is to apply a modulation with rows of a Hadamard matrix [38]–[40]. In this method, a periodic binary sequence, such as the MLBS, is used as a base signal. The second signal is obtained by adding, modulo 2, the sequence [0 1 0 1 ...] to the MLBS. The third signal is obtained by adding the sequence [0 0 1 1 0 0 1 1 ...] to the MLBS, and so on. Note that the sequence length of the ith orthogonal sequence is doubled compared with the length of the $(i-1)$th sequence.

Fig. 3 shows an example of two orthogonal binary sequences generated by the method. The length of the MLBS is 63 bits and generated at 1 kHz. The second sequence is known as an inverse-repeat sequence (IRS) because the modulation inverts every other digit of the MLBS. As shown in Fig. 3, the energy of every other harmonic has zero value in the IRS, which means that the MLBS and IRS have energy at different frequencies.

III. Setup Implementation

The PHIL setup shown in Fig. 5 at the DNV GL Flexible Power Grid Lab is made up of an Egston digital power amplifier and an OPAL-RT real-time digital simulator. The simulator is utilized to control the power amplifier, which consists of four groups of four single-phase units. The units

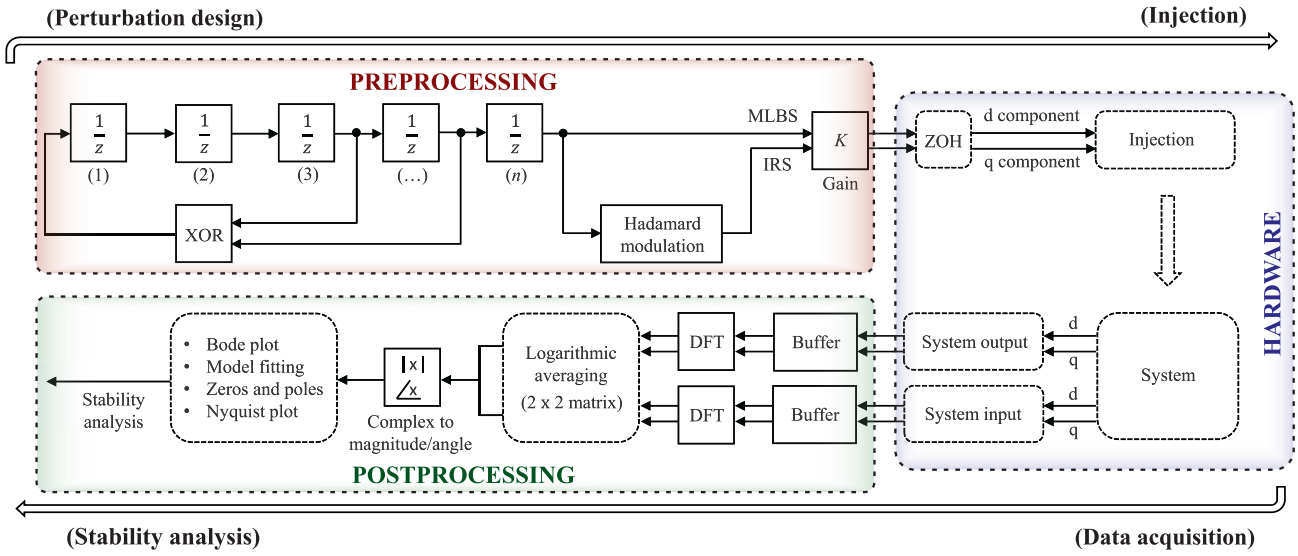

Fig. 4. Schematic of the preprocessing and postprocessing for the proposed real-time analysis method.

have a closed-loop bandwidth of 5 kHz and a total rated power of 200 kVA. The individual digital power amplifier unit is implemented with six interleaved parallel half-bridge converters that have an equivalent switching frequency of 125 kHz. For the closed-loop PHIL setup, the high-speed communication link is established between the real-time simulator and power amplifier. The current and voltage measurements are acquired from the output terminal of the digital amplifier to OPAL-RT every 4 μs, while the voltage and current control signal setpoints are sent to the Egston digital input/output box. A host PC is connected via asynchronous Ethernet to the OPAL-RT target PC. As shown in Fig. 5, the power amplifiers are isolated from the mains by a Dy transformer and 200-kW active front end. The power amplifiers can be freely configured to act as sources or loads depending on what kind of power system architecture is studied.

A. PHIL Implementation

Fig. 4 presents a schematic of the proposed real-time method for system stability analysis, which is implemented in OPAL-RT. The diagram consists of three sections: preprocessing, actual hardware, and postprocessing. The preprocessing section is responsible for the injection design and synthesis, where the orthogonal wideband perturbation signals are generated. The MLBS is implemented through shift registers and EXOR feedback, where the unit-delay blocks have a delay that corresponds to the generation frequency [41]. The orthogonal IRS is similarly generated in shift registers by processing the MLBS through the Hadamard modulation [32]. Then, the perturbations are simultaneously injected into the physical system to d- and q-components, and the input and output signals are continuously measured and buffered. The injection point is the current or voltage references of the device used in measurements; for example, the loop and grid impedance measurements are performed by superimposing the perturbation to the current reference of an inverter. In the postprocessing, the data sequences are Fourier-transformed and averaged by using (3) yielding the frequency-response data. The obtained frequency-response matrix is then (simultaneously) used to complete the Bode plot(s), Nyquist contour(s), system loop gains, and system poles and zeros. The refresh rate of the frequency-response matrix is pn/f_{g}, where P is the number of injection periods, N is the injection(s) length, and f_{g} is the injection(s) generation frequency. In this implementation, the postprocessing takes place in the OPAL-RT. In real implementations, however, the postprocessing can be integrated on the inverter controller structure, which also enables easy system scaling for a higher number of inverters, as the computational effort for an independent inverter is unchanged. Online techniques with similar computational demands have been successfully implemented on the converter controller hardware [20], [21], [42].

The designed perturbation signals are injected into the system through an adjustable gain (K). The optimal excitation amplitude depends on the system under measurement; for example, noise level and nonlinear behavior may deteriorate the measurement accuracy. In challenging measurement conditions, the excitation can be tuned to have more energy to ensure a sufficient signal-to-noise ratio. It is also possible to automatically or adaptively adjust the injection amplitude; for example, one can continuously measure the system total harmonic distortion (THD) and select the injection amplitude according to the THD limitations.

IV. Experiments and Analysis

A. Experimental Setup

A paralleled inverter system connected to a power grid was implemented using the PHIL setup (see Fig. 5). Fig. 6 shows a schematic of the system that consists of two inverters connected to a PCC. Each inverter consists of an amplifier unit, output filter, internal current controller, and phased-locked loop (PLL). Fig. 7 shows a detailed dq-domain control system of Inverter 1, where the injection and measured variables are highlighted with red. The filters were physically implemented by using a 0.5-mH three-phase inductor in Inverter 1 and 3.2-mH inductor in Inverter 2. The third amplifier group acts

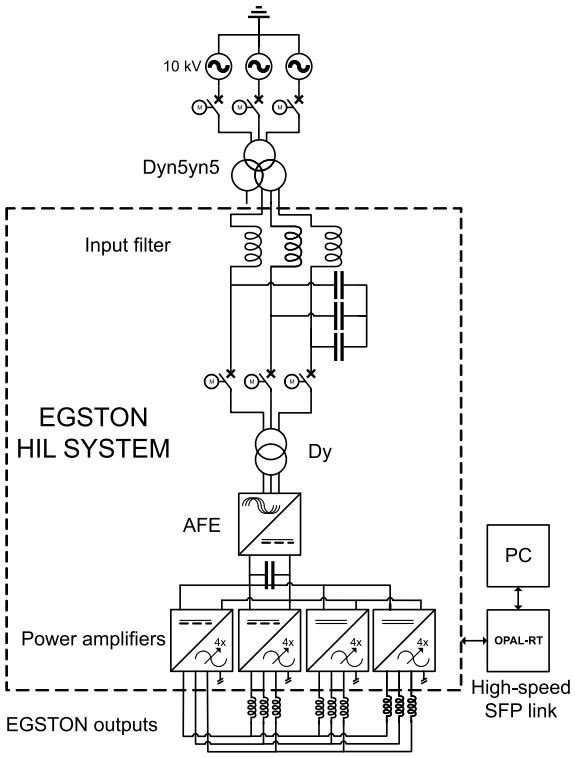

Fig. 5. PHIL setup in the DNV GL Flexible Power Grid Lab.

as a grid emulator, which provides the stiff grid voltages for the system and sinks the power from the inverters. An inductor of 1.0 mH was applied for the grid impedance emulation. The inverters operate at 50-kW total power. The detailed system parameters are shown in Table I.

B. Experimental Measurements

Two orthogonal binary perturbations were designed and applied in all experiments: the MLBS for measuring the desired d-current/voltage component (together with the cross-coupling component from d to q) and the IRS for measuring the desired q-current/voltage component (together with the cross-coupling component from q to d). The MLBS was synthesized using an 11-bit-length shift register. Thus, the MLBS was 2047-bit long, so it yielded a frequency resolution (i.e., the spacing between adjacent measured frequencies) of approximately 2.4 Hz. The length of the IRS was, by definition, twice the length of the MLBS. In each experiment, the MLBS and IRS were simultaneously injected into the system at 5 kHz. The injection amplitudes were adjusted such that output voltages and currents did not deviate from their nominal values by more than 5%. Considering the inherent harmonics present in most grids, the injection can be designed so that the decrease in power quality is negligible.

Three sets of experiments were performed to analyze the system stability in different conditions. In the experiments, the inverters' PLL bandwidth was tuned differently: in the first experiment, the bandwidth was set to 20 Hz, in the second experiment, to 60 Hz, and, finally, in the last experiment, to 85 Hz. As previously reported [43], increasing the PLL bandwidth in a weak grid generally decreases the system robustness, and altering the PLL tuning was chosen so that the proposed approach can be tested in versatile stability conditions. In all experiments, the full 2×2 frequency-response matrix, including the direct components (d and q) and cross-coupling components (dq and qd), was measured.

The experiments were performed by first utilizing the inverters in measurements (Injection Points 1 and 2 in Fig. 6) and then performing the grid measurements (Injection Point 3). The injection point in the inverter measurements allows measuring both the current-controller loop gains and grid impedance simultaneously with the same injection. As a consequence, this process eliminates the need for separate measurements for loop gains and grid impedance. In the loop gain measurements, the input vector is the current-controller reference $\mathbf{i}_{\text{in}} = [i_{\text{in-d}},\ i_{\text{in-d}}]^T$, and the output vector is the current response $\mathbf{i}_o = [i_{\text{d}},\ i_{\text{q}}]^T$ (as shown in Fig. 7). Similarly, in the grid impedance measurements, the output current $\mathbf{i}_o$ is the excitation, and the output vector is the voltage response $\mathbf{v}_{\text{pcc}} = [v_{\text{d}},\ v_{\text{q}}]^T$. The measurements are sampled at 10 kHz, and the impedances and loop gains are extracted from the measured signals by applying (1)–(3) to each input/output pair. In order to avoid spectral leakage, the measured signals are segmented to consist of 4094 samples for the MLBS-perturbed signals and 8188 samples for the IRS-perturbed signals (as the sampling frequency is twice as high as the generation frequency of the perturbations). First, Inverter 2 was disconnected, and the loop and impedance measurements were performed with Inverter 1. After this, Inverter 2 was reconnected, and the injection was applied to Injection Point 2 to obtain the current control loop of the second inverter. It would have been possible to simultaneously measure the current loop gains from both inverters, but this approach would have required the use of four orthogonal sequences. Finally, the injections were applied to Injection Point 3 for obtaining the aggregated output impedance of the paralleled inverters. In all measurements, (1) was applied over 100 injection periods for the MLBS and over 50 injection periods for the IRS (as the length of the IRS is doubled compared with the MLBS). The refreshment rate, which is equal to the duration of the averaged measurement cycle, is 41 s during which the computation is performed. With modern inverter controllers, transfer function calculation and stability analysis can be easily performed within this time frame, enabling real-time stability assessment. When very fast (millisecond range) measurement cycles are applied, the computational requirements become stricter, and the hardware performance must be considered in the method tuning.

Fig. 8 shows the measured inverters' aggregated output impedance and the grid impedance at the PCC for all the three different experiments. A simple approximate of the system robustness can be obtained by examining the qq-component of the impedances, where the phase margin at the intersection frequency indicates system stability margins. For the system with 20-Hz PLL bandwidths, the phase margin is approximately 57Â° at the intersection frequency around 190 Hz. Increasing the bandwidth to 60 Hz reduces the phase margin to 13Â° and increasing to 85 Hz decreases the phase margin to 4Â°, indicating almost marginal stability. However, this single-input–single-output consideration ignores the inherent

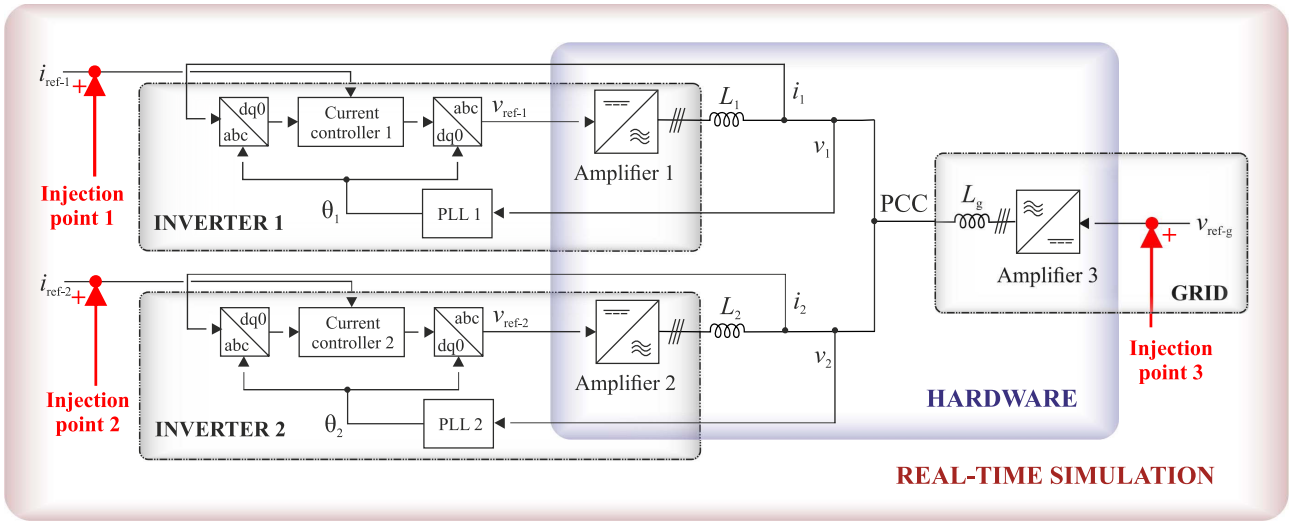

Fig. 6. Conceptual diagram of the experimental setup.

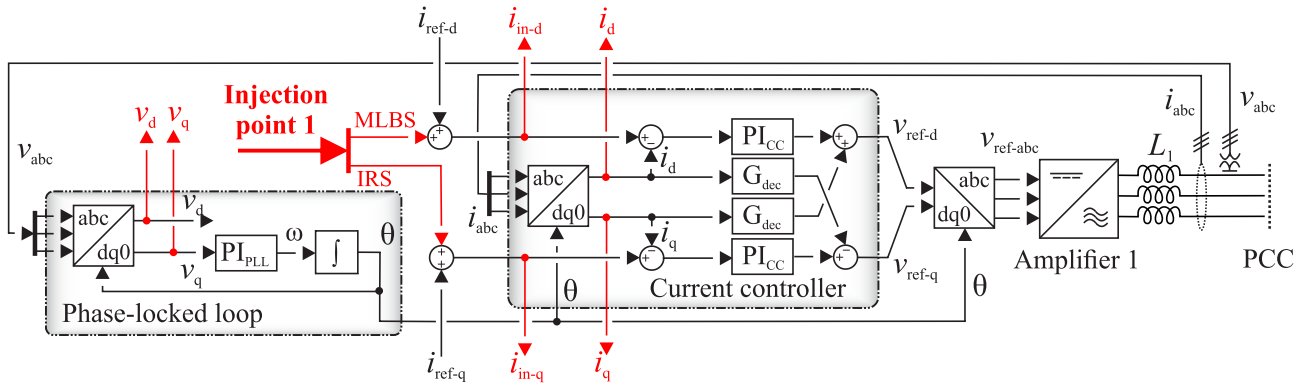

Fig. 7. Detailed control diagram and injection schematic of Inverter 1.

TABLE I
PARAMETERS OF THE EXPERIMENTAL SETUP

Parameter	Symbol	Value
Grid frequency	f_g	50 Hz
Nominal main voltage (RMS)	V_n	400 V
Output power of inverters	P_{sp}	24.4 kW
Power factor of inverters	$\cos(\phi)$	1.00
D-current reference	i_d^*	50 A
Grid inductance	L_g	2.0 mH
Inverter 1 L-filter inductance	L_1	0.5 mH
Inverter 2 L-filter inductance	L_2	3.2 mH
Inverter 1 CC proportional gain	$K_{CC1\text{-}P}$	1.6514
Inverter 1 CC integral gain	$K_{CC1\text{-}I}$	518.8
Inverter 2 CC proportional gain	$K_{CC2\text{-}P}$	10.070
Inverter 2 CC integral gain	$K_{CC2\text{-}I}$	3162
20 Hz PLL proportional gain	$K_{PLL20\text{-}P}$	1.30
20 Hz PLL integral gain	$K_{PLL20\text{-}I}$	75.2
60 Hz PLL proportional gain	$K_{PLL60\text{-}P}$	3.90
60 Hz PLL integral gain	$K_{PLL60\text{-}I}$	676.4
85 Hz PLL proportional gain	$K_{PLL85\text{-}P}$	5.52
85 Hz PLL integral gain	$K_{PLL85\text{-}I}$	1358

multivariable nature of the system, and the reliable analysis requires the use of complete 2×2 matrices [6], which is presented in Section IV-C. Similarly, the 2×2 matrices of the load-affected internal current control loops are shown in Fig. 9 for Inverter 1 and in Fig. 10 for Inverter 2.

C. Stability Analysis

The stability analysis can be performed on the measured PCC impedances or internal loop gains, where similar methods can be applied. In this work, the stability analysis is performed by generalized Nyquist criterion (GNC) for the impedances and pole–zero fittings for the internal loop gains. These methods can be applied simultaneously, as the measurements can be obtained with a single injection cycle as discussed previously. In the GNC, the distance from the eigenvalue contour to the critical point shows the system's robustness. Fig. 11 presents the eigenvalue contours for the system for different experiments. A drastic change toward instability is seen when the PLL bandwidth is increased as the eigenvalue 1 contour shifts toward the critical point. With 85-Hz PLL bandwidth, the system is almost marginally stable.

In addition to the impedance-based GNC analysis, the system stability was analyzed through system poles and zeros. The poles and zeros were continuously calculated from the same impedance data and, additionally, the internal current-controller loops for each inverter. Consequently, the method enabled the use of two parallel approaches.

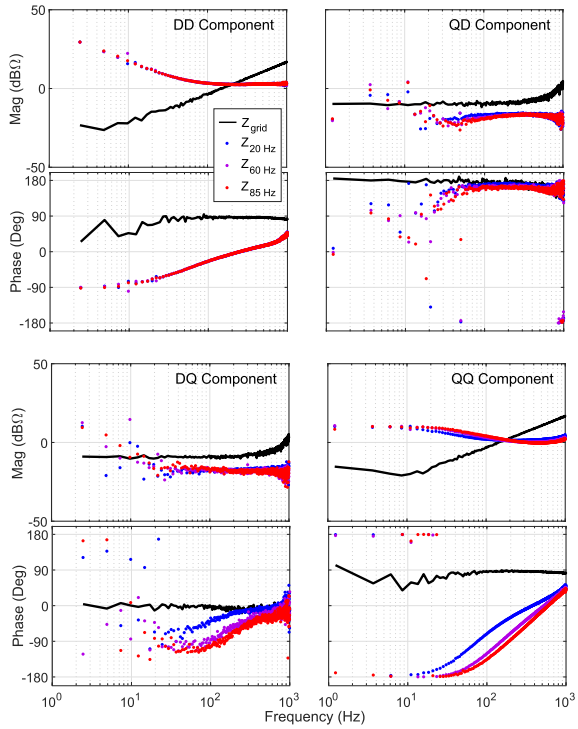

Fig. 8. Measured impedances of the grid (black) and the inverters with different PLL bandwidth tunings.

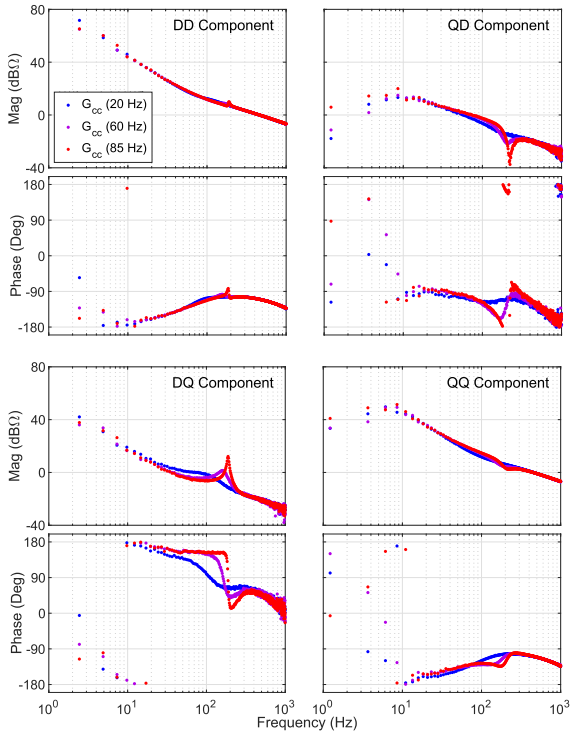

Fig. 10. Measured Inverter 2 current-controller loop gain with different PLL tunings.

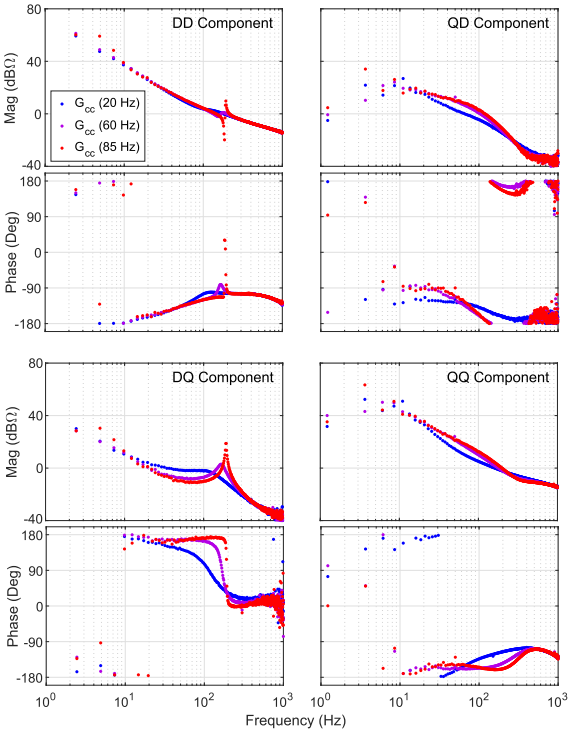

Fig. 9. Measured Inverter 1 current-controller loop gain with different PLL tunings.

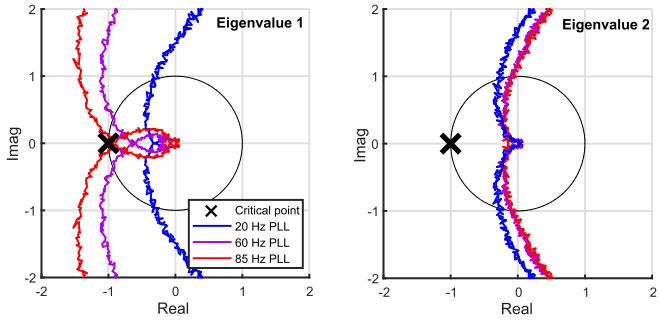

Fig. 11. Impedance-based Nyquist contours with different PLL tunings.

For evaluating the values of zeros and poles, parametric models were continuously estimated based on the measured loop gains [44]. Fig. 12 shows the estimated poles and zeros based on the minor loop (impedance ratio) and loop gains from Inverters 1 and 2. The critical poles shown in the bottom right subfigure shift toward the imaginary axis, and approximately, the same stability margins can be obtained through all the methods.

The use of parallel approaches increases the flexibility and usability of the stability analysis method, as both approaches have their advantages. The impedance-based approach excels in system-level analysis and monitoring but becomes more time-consuming in very complex systems with many inverters. On the other hand, the loop-gain-based analysis is readily available even in such systems and, additionally, provides detailed information on the individual-inverter level. This local data can be utilized in, for example, fault prevention by identifying the low-stability devices or in independent adaptive control of the inverters.

D. Time-Domain Verification

The presented methods assess the stability in the frequency domain, as the frequency-domain results are significantly more straightforward to derive. However, ultimately, the interest in

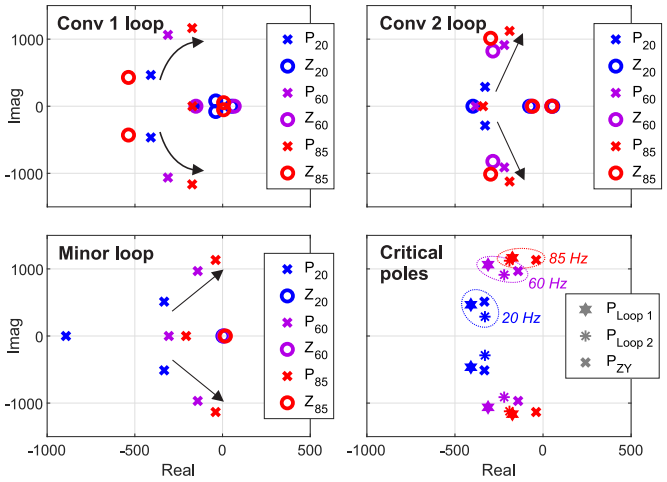

Fig. 12. Pole–zero maps based on measured minor loop gain and inverter current-controller loops.

system performance often relies on the time-domain operation, and the frequency domain is applied as an auxiliary domain. In order to validate the obtained stability margins and to verify the proposed methodology, a comparison between the transient performance of the actual system and the predicted stability margins is performed in the time domain. In the following analysis, the minor loop (impedance ratio) poles and zeros were used to construct the corresponding dynamics in the time domain by predicting the time-domain step response from the obtained frequency-domain margins. The validation was performed offline by first constructing transfer functions from the pole–zero data (as shown in (4) in the footnote for the 85-Hz PLL system). Then, the time-domain prediction was obtained by applying MATLAB step-function on the pole–zero data, where the step response of a transfer function is calculated numerically. The calculated response is compared with the actual response of the experimental system shown in Fig. 6

Fig. 13 presents the predicted system behavior and the actual response to a step change in the current reference of the Inverter 1. The q-channel current reference is changed from -10 to 10 A, and the response is measured for all the test parameter sets. The figure shows that the actual system response is very accurately predicted with the proposed method, as both the oscillatory frequency and the damping ratio closely match the experimental waveform. A steady-state error that persists after the oscillations have settled results from the minor deviations in the fit locations of the poles and zeros, which accumulate to the dc-gain of the system. From the stability perspective, the significant characteristics that quantify the system stability are the overshoot, oscillatory frequency, and the damping ratio (that is, the rate of decay in the oscillations). With the proposed methods, these were

$$G(s) = \frac{2.03\text{e}05 * (s + 3.57\text{e}03)(s + 1.99\text{e}03)}{(s + 1.31\text{e}06)(s + 3.89\text{e}01 + j1.15\text{e}03)(s + 3.89\text{e}01 - j1.15\text{e}03)} = \frac{2.03\text{e}05s^2 + 1.13\text{e}09s + 1.45\text{e}12}{s^3 + 1.31\text{e}06s^2 + 1.03\text{e}08s + 1.74\text{e}12}. \quad (4)$$

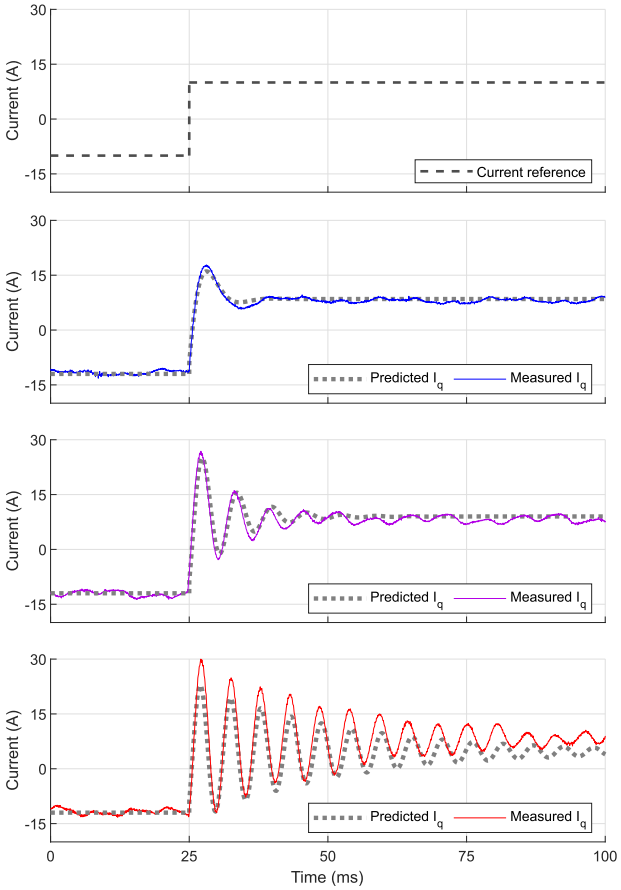

Fig. 13. Step response comparison.

accurately predicted even for the system that was close to marginal stability.

V. Conclusion

Paralleled inverters play an important role in the operation of the most grid-connected system. A number of stability issues arise from the interactions among multiple inverter subsystems and the power grid. Recent studies have presented techniques, such as impedance-based analysis, to assess the stability and dynamic characteristics of multi-inverter systems. Frequency-response measurements are often required to extract information from these systems, as the internal dynamics of some subsystems may be unknown. Especially, online methods for measurements are highly desirable, in order to provide real-time data on the system status, which can be utilized in advanced system monitoring, fault protection, and adaptive control. This article has presented a practical real-time approach to perform a comprehensive stability analysis of a three-phase grid-connected system containing paralleled inverters by applying a PHIL platform. The method applies orthogonal injections for multivariable system identification and utilizes parallel approaches for the stability analysis by applying impedance-based analysis and loop-gain assessment simultaneously. Consequently, detailed information can be obtained from both local and global points of view for holistic stability assessment. Experimental measurements were shown from a high-power energy distribution system recently developed at DNV GL. The presented methods can be used

to modify various system characteristics, such as impedance behavior and control dynamics, in real time, thereby providing means for several stability and adaptive control design tools for grid-connected systems containing paralleled inverters.

ACKNOWLEDGMENT

This research and testing have been performed using the ERIGrid Research Infrastructure. The support of the European Research Infrastructure ERIGrid and its partner DNVGL is very much appreciated.

REFERENCES

[1] R. R. Karasani, V. B. Borghate, P. M. Meshram, H. M. Suryawanshi, and S. Sabyasachi, "A three-phase hybrid cascaded modular multilevel inverter for renewable energy environment," *IEEE Trans. Power Electron.*, vol. 32, no. 2, pp. 1070–1087, Feb. 2017.

[2] T. Windisch and W. Hofmann, "A novel approach to MTPA tracking control of AC drives in vehicle propulsion systems," *IEEE Trans. Veh. Technol.*, vol. 67, no. 10, pp. 9294–9302, Oct. 2018.

[3] F. Z. Peng, "Flexible AC transmission systems (FACTS) and resilient AC distribution systems (RACDS) in smart grid," *Proc. IEEE*, vol. 105, no. 11, pp. 2099–2115, Nov. 2017.

[4] V. Madonna, P. Giangrande, and M. Galea, "Electrical power generation in aircraft: Review, challenges, and opportunities," *IEEE Trans. Transport. Electrific.*, vol. 4, no. 3, pp. 646–659, Sep. 2018.

[5] W. Liu *et al.*, "Power quality assessment in shipboard microgrids under unbalanced and harmonic AC bus voltage," *IEEE Trans. Ind. Appl.*, vol. 55, no. 1, pp. 765–775, Jan. 2019.

[6] T. Suntio *et al.*, "Impedance-based interactions in grid-tied three-phase inverters in renewable energy applications," *Energies*, vol. 12, no. 3, p. 464, Jan. 2019.

[7] C. Li, "Unstable operation of photovoltaic inverter from field experiences," *IEEE Trans. Power Del.*, vol. 33, no. 2, pp. 1013–1015, Apr. 2018.

[8] H. Liu *et al.*, "Subsynchronous interaction between direct-drive PMSG based wind farms and weak AC networks," *IEEE Trans. Power Syst.*, vol. 32, no. 6, pp. 4708–4720, Nov. 2017.

[9] L. Wang, X. Xie, Q. Jiang, H. Liu, Y. Li, and H. Liu, "Investigation of SSR in practical DFIG-based wind farms connected to a series-compensated power system," *IEEE Trans. Power Syst.*, vol. 30, no. 5, pp. 2772–2779, Sep. 2015.

[10] H. Alenius and T. Roinila, "Impedance-based stability analysis of paralleled grid-connected rectifiers: Experimental case study in a data center," *Energies*, vol. 13, no. 8, p. 2109, Apr. 2020.

[11] E. A. A. Coelho, P. C. Cortizo, and P. F. D. Garcia, "Small-signal stability for parallel-connected inverters in stand-alone AC supply systems," *IEEE Trans. Ind. Appl.*, vol. 38, no. 2, pp. 533–542, May 2002.

[12] J. L. Agorreta, M. Borrega, J. López, and L. Marroyo, "Modeling and control of *N* -paralleled grid-connected inverters with LCL filter coupled due to grid impedance in PV plants," *IEEE Trans. Power Electron.*, vol. 26, no. 3, pp. 770–785, Mar. 2011.

[13] M. Lu, X. Wang, F. Blaabjerg, and P. C. Loh, "An analysis method for harmonic resonance and stability of multi-paralleled LCL-filtered inverters," in *Proc. IEEE 6th Int. Symp. Power Electron. for Distrib. Gener. Syst. (PEDG)*, Jun. 2015, pp. 1–6.

[14] J. Sun, "Impedance-based stability criterion for grid-connected inverters," *IEEE Trans. Power Electron.*, vol. 26, no. 11, pp. 3075–3078, Nov. 2011.

[15] T. Roinila and T. Messo, "Online grid-impedance measurement using ternary-sequence injection," *IEEE Trans. Ind. Appl.*, vol. 54, no. 5, pp. 5097–5103, Sep. 2018.

[16] M. Amin and M. Molinas, "Small-signal stability assessment of power electronics based power systems: A discussion of Impedance- and eigenvalue-based methods," *IEEE Trans. Ind. Appl.*, vol. 53, no. 5, pp. 5014–5030, Sep. 2017.

[17] F. Cavazzana, P. Mattavelli, M. Corradin, and I. Toigo, "On the stability analysis of multiple parallel inverters using the impedance multiplication effect," in *Proc. 8th IET Int. Conf. Power Electron., Mach. Drives (PEMD)*, 2016, pp. 1–6.

[18] H. Alenius, M. Berg, R. Luhtala, and T. Roinila, "Stability and performance analysis of grid-connected inverter based on online measurements of current controller loop," in *Proc. 45th Annu. Conf. Ind. Electron. Soc.*, Oct. 2019, pp. 2013–2019.

[19] B. K. Bose, "Global energy scenario and impact of power electronics in 21st century," *IEEE Trans. Ind. Electron.*, vol. 60, no. 7, pp. 2638–2651, Jul. 2013.

[20] A. Barkley and E. Santi, "Online monitoring of network impedances using digital network analyzer techniques," in *Proc. 24th Annu. IEEE Appl. Power Electron. Conf. Expo.*, Feb. 2009, pp. 440–446.

[21] A. Riccobono, M. Mirz, and A. Monti, "Noninvasive online parametric identification of three-phase AC power impedances to assess the stability of grid-tied power electronic inverters in LV networks," *IEEE J. Emerg. Sel. Topics Power Electron.*, vol. 6, no. 2, pp. 629–647, Jun. 2018.

[22] A. Merabet, K. A. Tawfique, M. A. Islam, S. Enebeli, and R. Beguenane, "Wind turbine emulator using OPAL-RT real-time HIL/RCP laboratory," in *Proc. 26th Int. Conf. Microelectron. (ICM)*, Dec. 2014, pp. 192–195.

[23] E. Breaz, F. Gao, D. Paire, and R. Tirnovan, "Fuel cell modeling with dSPACE and OPAL-RT real time platforms," in *Proc. IEEE Transp. Electrific. Conf. Expo. (ITEC)*, Jun. 2014, pp. 1–6.

[24] D. Bian, M. Kuzlu, M. Pipattanasomporn, S. Rahman, and Y. Wu, "Real-time co-simulation platform using OPAL-RT and OPNET for analyzing smart grid performance," in *Proc. IEEE Power Energy Soc. Gen. Meeting*, Jul. 2015, pp. 1–5.

[25] P. C. Kotsampopoulos, F. Lehfuss, G. F. Lauss, B. Bletterie, and N. D. Hatziargyriou, "The limitations of digital simulation and the advantages of PHIL testing in studying distributed generation provision of ancillary services," *IEEE Trans. Ind. Electron.*, vol. 62, no. 9, pp. 5502–5515, Sep. 2015.

[26] C. Yin, B. Ye, X. Wang, and L. Dai, "Power hardware-in-the-loop simulation of a distributed generation system connected to a weak grid," in *Proc. IEEE Conf. Energy Internet Energy Syst. Integr. (EI2)*, Nov. 2017, pp. 1–6.

[27] H. Alenius, T. Messo, T. Reinikka, and T. Roinila, "Aggregated modeling and power hardware-in-the-loop emulation of grid impedance," in *Proc. IEEE Energy Convers. Congr. Expo. (ECCE)*, Sep. 2018, pp. 4179–4186.

[28] T. Reinikka, H. Alenius, T. Roinila, and T. Messo, "Power hardware-in-the-loop setup for stability studies of grid-connected power converters," in *Proc. Int. Power Electron. Conf. (IPEC-Niigata -ECCE Asia)*, May 2018, pp. 1704–1710.

[29] T. Suntio, T. Messo, and J. Puukko, *Converters: Dynamics and Control in Conventional and Renewable Energy Applications*. Hoboken, NJ, USA: Wiley, 2017.

[30] L. Harnefors, "Modeling of three-phase dynamic systems using complex transfer functions and transfer matrices," *IEEE Trans. Ind. Electron.*, vol. 54, no. 4, pp. 2239–2248, Aug. 2007.

[31] R. Pintelon and J. Schoukens, *System Identification—A Frequency Domain Approach*. New York, NY, USA: The Institute of Electrical and Electronics Engineers, 2001.

[32] A. Tan and K. Godfrey, *Industrial Process Identification—Perturbation Signal Design and Applications*. Cham, Switzerland: Springer, 2019.

[33] T. Roinila, M. Vilkko, and J. Sun, "Broadband methods for online grid impedance measurement," in *Proc. IEEE Energy Convers. Congr. Expo.*, Sep. 2013, pp. 3003–3010.

[34] T. Roinila, H. Abdollahi, S. Arrua, and E. Santi, "Adaptive control of DC power distribution systems: Applying pseudo-random sequences and Fourier techniques," in *Proc. Int. Power Electron. Conf. (IPEC-Niigata -ECCE Asia)*, May 2018, pp. 1719–1723.

[35] A. Riccobono *et al.*, "Stability of shipboard DC power distribution: Online impedance-based systems methods," *IEEE Electrific. Mag.*, vol. 5, no. 3, pp. 55–67, Sep. 2017.

[36] H. Abdollahi, S. Arrua, T. Roinila, and E. Santi, "A novel DC power distribution system stabilization method based on adaptive resonance-enhanced voltage controller," *IEEE Trans. Ind. Electron.*, vol. 66, no. 7, pp. 5653–5662, Jul. 2019.

[37] R. Luhtala, H. Alenius, T. Messo, and T. Roinila, "Online frequency response measurements of grid-connected systems in presence of grid harmonics and unbalance," *IEEE Trans. Power Electron.*, vol. 35, no. 4, pp. 3343–3347, Apr. 2020.

[38] T. Roinila, T. Messo, and E. Santi, "MIMO-identification techniques for rapid impedance-based stability assessment of three-phase systems in DQ domain," *IEEE Trans. Power Electron.*, vol. 33, no. 5, pp. 4015–4022, May 2018.

[39] R. Luhtala, T. Roinila, and T. Messo, "Implementation of real-time impedance-based stability assessment of grid-connected systems using MIMO-identification techniques," *IEEE Trans. Ind. Appl.*, vol. 54, no. 5, pp. 5054–5063, Sep. 2018.

[40] T. Roinila, H. Abdollahi, S. Arrua, and E. Santi, "Real-time stability analysis and control of multiconverter systems by using MIMO-identification techniques," *IEEE Trans. Power Electron.*, vol. 34, no. 4, pp. 3948–3957, Apr. 2019.

[41] K. Godfrey, *Perturbation Signals for System Identification*. Upper Saddle River, NJ, USA: Prentice-Hall, 1993.

[42] T. Roinila, H. Abdollahi, S. Arrua, and E. Santi, "Online measurement of bus impedance of interconnected power electronics systems: Applying orthogonal sequences," in *Proc. IEEE Energy Convers. Congr. Expo. (ECCE)*, Oct. 2017, pp. 5783–5788.

[43] T. Messo, J. Jokipii, A. Makinen, and T. Suntio, "Modeling the grid synchronization induced negative-resistor-like behavior in the output impedance of a three-phase photovoltaic inverter," in *Proc. 4th IEEE Int. Symp. Power Electron. Distrib. Gener. Syst. (PEDG)*, Jul. 2013, pp. 1–7.

[44] L. Ljung, *System Identification-Theory for the User*. Upper Saddle River, NJ, USA: Prentice-Hall, 1999.

Henrik Alenius (Member, IEEE) received the M.Sc. degree in electrical engineering from the Tampere University of Technology, Tampere, Finland, in 2018. He is currently pursuing the Ph.D. degree with the Faculty of Information Technology and Communication Sciences, Tampere University, Tampere.

His research interests include impedance-based interactions in grid-connected systems, broadband methods in impedance measurements, and the stability analysis of multiparallel inverters.

Tomi Roinila (Member, IEEE) received the M.Sc. (Tech.) and Dr.Tech. degrees in automation and control engineering from the Tampere University of Technology, Tampere, Finland, in 2006 and 2010, respectively.

He is currently an Associate Professor with the Faculty of Information Technology and Communications Sciences, Tampere University, Tampere. His main research interests include modeling and control of grid-connected power-electronics systems, and modeling of multiconverter systems.

Roni Luhtala (Member, IEEE) received the M.Sc. degree in electrical engineering from the Tampere University of Technology, Tampere, Finland, in 2017. He is currently pursuing the Ph.D. degree with the Faculty of Engineering and Natural Sciences, Tampere University, Tampere.

His main research interests include real-time identification and adaptive control of grid-connected systems.

Tuomas Messo (Member, IEEE) received the Dr.Tech. degree in electrical engineering from the Tampere University of Technology, Tampere, Finland, in 2014.

He is currently with GE Grid Solutions, Tampere. He is also an Adjunct Professor of power electronics with Tampere University, Tampere, where he was an Assistant Professor from 2016 to 2019. His research interests include grid-connected three-phase power converters for renewable energy applications and microgrids, dynamic modeling, control design, impedance-based interactions in three-phase systems, and impedance design of grid-connected inverters.

Andrew Burstein (Member, IEEE) received the B.S. degree *(cum laude)* in electrical engineering technology: smart grids from the State University College of New York at Buffalo, Buffalo, NY, USA, in 2013, and the M.Sc. degree *(cum laude)* in sustainable energy technology from the Eindhoven University of Technology, Eindhoven, The Netherlands, in 2015.

He is currently a Researcher with DNV GL Power and Renewables, Arnhem, The Netherlands. His main focus is working in the Flex Power Grid Laboratory and is interested in developing leading cutting edge testing services for grid-connected power electronics.

Erik de Jong (Senior Member, IEEE) received the B.Ing. and M.Ing. degrees *(cum laude)* in electric and electronic engineering from Rand Afrikaans University, Johannesburg, South Africa, in 2001 and 2003, respectively, and the Ph.D. degree from the Delft University of Technology, Delft, The Netherlands, in 2007.

Since 2007, he has been with DNV GL/Energy, Arnhem, The Netherlands, as a technical professional, specializing and providing consultancy services in power electronics and its applications in utility grids. Since 2008, he has been with the Flex Power Grid Laboratory as a General Manager responsible for all operations regarding medium-voltage grid inverter research, testing, and certification. Since 2013, he has been a Senior Researcher in power electronics and power cybernetics with the Strategic Research and Innovation Department, DNV GL. As a part-time Associate Professor at the Electrical Energy Systems Group, Eindhoven University of Technology, Eindhoven, The Netherlands, he directs research programs and guides Ph.D. students in the field of power electronics dominated (smart) grids. He is very active in publishing scientific research results in peer-reviewed international conferences and journals.

Dr. de Jong received the prestigious Hidde Nijland Award in 2010 for his contributions in the field of testing utility-interactive power electronics. He serves as an Expert in the IEC 61400-21 Standardisation Maintenance Team (TC88) for revision 3 on Power Quality and is an Industry Member of the DERLab Association and the Dutch Delegate of the Smart Grid International Research Facility Network (IEA-ISGAN-SIRFN) Activities.

Alejandra Fabian received the B.Sc. degree in electronics technology from the Monterrey Institute of Technology and Higher Education, Monterrey, Mexico, in 2011, and the M.Sc. degree in sustainable energy technology from the Eindhoven University of Technology, Eindhoven, The Netherlands, in 2016.

She is currently a Researcher with DNV GL Group Technology & Research, Arnhem, The Netherlands. Her research interests are in hardware-in-the-loop methods, power systems, and control applications for renewable energy integration.